

Dark and baryonic matter in the MareNostrum Universe

S. Gottlöber*, G. Yepes[†], A. Khalatyan*, R. Sevilla[†] and V. Turchaninov**

*Astrophysical Institute Potsdam, An der Sternwarte 16, 14482 Potsdam, Germany

[†]Grupo de Astrofísica, Universidad Autónoma de Madrid, Madrid E-28049, Spain

**Keldysh Institute for Applied Mathematics, Miusskaja Ploscad 4, 125047 Moscow, Russia

Abstract. We report some results from one of the largest hydrodynamical cosmological simulations of large scale structures that has been done up to date. The *MareNostrum Universe* SPH simulation consists of 2 billion particles (2×1024^3) in a cubic box of $500 h^{-1}$ Mpc on a side. This simulation has been done in the MareNostrum parallel supercomputer at the Barcelona SuperComputer Center. Due to the large simulated volume and good mass resolution, our simulated catalog of dark matter halos comprises more than half a million objects with masses larger than a typical Milky Way galaxy halo. From this dataset we have studied several statistical properties such as the halo mass function, the distribution of shapes of dark and gas components within halos, the baryon fraction, cumulative void volume etc. This simulation is particularly useful to study the large scale distribution of baryons in the universe as a function of temperature and density. In this paper we also show the time evolution of the gas fractions at large scales.

INTRODUCTION

During the last couple of decades the exciting observational developments have enormously increased our knowledge about the history of the universe. A comparable progress has been made in our theoretical understanding of the main processes that govern the evolution of structure in the Universe. A substantial part of this progress is due to the increasing possibilities to simulate the formation and evolution of structure on different scales using the new generation of massive parallel supercomputers.

The standard model of cosmological structure formation is based on the idea of an early inflationary phase of the evolution of the Universe. According to the simplest models of inflation during this phase fluctuations with a scale free power spectrum have been created. On large scales this power spectrum has been observed with high accuracy by the WMAP satellite [8] which measured the fluctuations in the Cosmic Microwave Background radiation. The cosmological models are characterized by only five parameters: the current rate of universal expansion, H_0 , the mass density parameter, Ω_{mat} , the value of the cosmological constant, Ω_{Λ} , the primordial baryon abundance, Ω_b , and the overall normalization of the power spectrum of initial density fluctuations, typically characterized by σ_8 , the present-day rms mass fluctuations on spheres of radius $8h^{-1}$ Mpc.

Since 85 % of the matter consists of dark matter particles the gravitational evolution of the structures in the universe is dominated by the dark matter. Many codes follow only the dark matter clumping during cosmological evolution (e.g. [10]). But most of

the information we get from the Universe comes from the baryons (either in the form of X-ray emitting gas, or from the stars). If one is interested in studying the distribution of baryons on large scales then gas dynamics must be added to the gravitational evolution in a cosmological simulation. This is not a trivial issue because gasdynamical processes are very costly to simulate once the gas is compressed to high densities when it falls into the potential wells of the dark matter distribution.

Thanks to the recent advances in massively parallel computing, and to the development of efficient MPI parallel codes that can use the total computing power of thousand of processors linked together, numerical simulations can treat more and more particles to describe the two main components of the universe (collisionless dark matter and gas). This allows to simulate larger and larger computational volumes with enough resolution to identify typical galaxies like the Milky Way.

To compare the large scale distribution of dark matter and gas we have been able to perform one of the largest cosmological gasdynamical simulations ever done so far. We have followed the nonlinear evolution of both the dark matter and the gas component within an 'adiabatic', namely non-radiative and non-dissipative, cosmological Smooth Particle Hydrodynamical (SPH) simulation. In what follows we will describe the main features of the numerical simulation and will discuss some of the results of the analyses we are doing in the large simulated dataset.

NUMERICAL SIMULATION

In our numerical simulation we have assumed the spatially flat concordance cosmological model with the parameters $\Omega_m = 0.3$, $\Omega_{bar} = 0.045$, $\Omega_\Lambda = 0.7$, the normalization $\sigma_8 = 0.9$ and the slope $n = 1$ of the power spectrum. Within a box of $500h^{-1}\text{Mpc}$ size the linear power spectrum at redshift $z = 40$ has been represented by 1024^3 DM particles of mass $m_{DM} = 8.3 \times 10^9 h^{-1} M_\odot$ and 1024^3 gas particles of mass $m_{gas} = 1.5 \times 10^9 h^{-1} M_\odot$. The nonlinear evolution of structures has been followed by the GADGET II code of V. Springel [9]. For the gravitational evolution we have used the TREEPM algorithm on a homogeneous Eulerian grid to compute large scale forces by the Particle-Mesh algorithm. In this simulation we employed 1024^3 mesh points to compute the density field from particle positions and FFT to derive gravitational forces. Since the baryonic component is also discretized by the gas particles all hydrodynamical quantities have to be determined using interpolation from the gas particles. Within GADGET the equations of gas dynamics are solved by means of the Smoothed Particle Hydrodynamics method in its entropy conservation scheme. To follow structure formation until redshift $z = 0$ we have restricted ourselves to the gas-dynamics without including dissipative or radiative processes or star formation. The spatial force resolution was set to an equivalent Plummer gravitational softening of $15 h^{-1}$ comoving kpc. The SPH smoothing length was set to the distance to the 40^{th} nearest neighbor of each SPH particle. In any case, we do not allow smoothing scales to be smaller than the gravitational softening of the gas particles. Using for three weeks 512 processors of the MareNostrum supercomputer at BSC Barcelona (this time corresponds to 29 CPU years) we have finished the simulation and created the *MareNostrum Universe*.

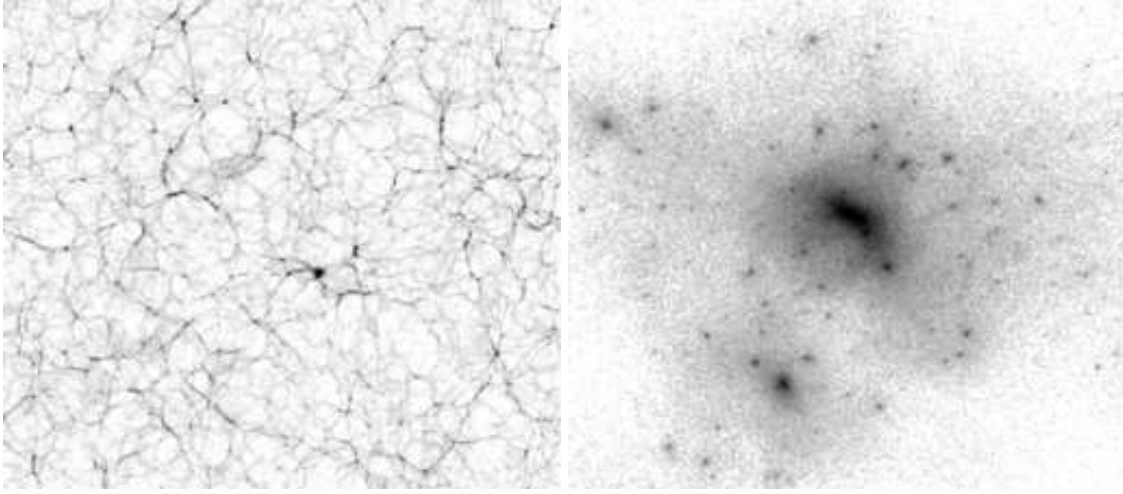


FIGURE 1. Left: The slice through the simulation contains the second most massive cluster found in the box at redshift $z = 0$. Right: Zoom-in on this cluster. The size of the box is $20 h^{-1}\text{Mpc}$. Substructures can be clearly seen.

In Fig. 1 we show on the left a slice through the simulation showing the density distribution of the dark matter component. One can clearly see the large-scale filamentary structure. Approximately in the center of the slice at the intersection of a few massive filaments one can see the second most massive cluster in the simulation. Its total virial mass (baryons and dark matter) is $2.2 \times 10^{15} h^{-1} M_{\odot}$ with a virial radius of $2.6 h^{-1} \text{Mpc}$. On the right hand side we show a zoom-in on this cluster where the substructures can be seen.

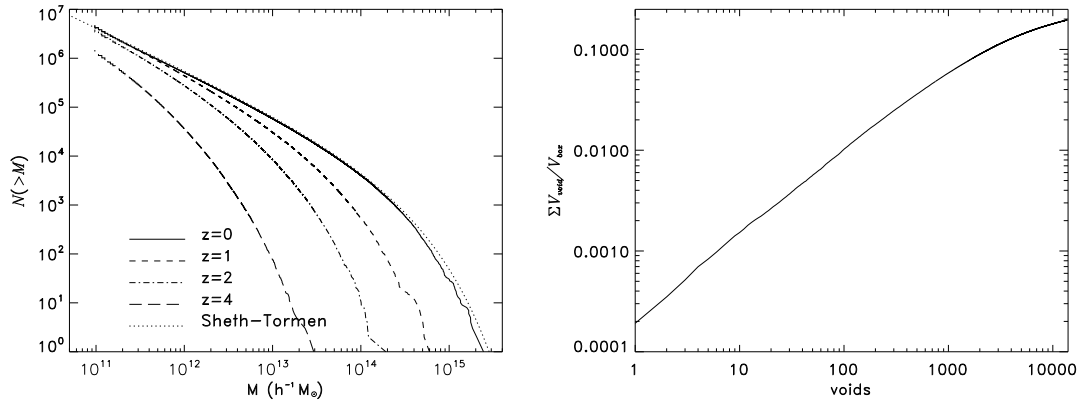


FIGURE 2. Left: Mass function of halos at redshift $z = 0, 1, 2, 4$ and Sheth-Tormen mass function (dotted line) at redshift $z = 0$. Right: Cumulative volume occupied by voids

Halos

Gravitationally bound halos of different mass form has been formed during the cosmological evolution. These halos consist of dark matter and gas. Due to the hydrodynamical interaction of the gas in general the ration of gas to dark matter within the halos is different from the mean ratio of 0.15 assumed in the simulation. Moreover, the spatial distribution of gas and dark matter differ inside the halos. Even if one can see the halos my naked eye as white spots in Fig. 1 it is a challenge to identify numerically all those halos within the distribution of two billion particles and to determine their properties.

For this purpose we have developed a parallel version of the hierarchical friends-of-friends (FOF) algorithm described in [7]. The FOF algorithm bases on the minimal spanning tree (MST) of the particle distribution. The minimal spanning tree of any point distribution is a unique well defined quantity which describes the clustering properties of the point process completely [2]. The minimal spanning tree of n points contains $n - 1$ connections. Based on the minimum spanning tree we sort the particles in such a way that we get a cluster-ordered sequence $P = \{p_1, p_2, \dots, p_n\}$. Any particle cluster is a segment of the sequence P , i.e. it consist of points p_i, p_{i+1}, \dots, p_j for some indexes i and j . Neighboring clusters, i.e. clusters which merged immediately after increasing r , are neighboring segments on P . Let us denote the length at which clusters p_i, p_{i+1}, \dots, p_j and $p_{j+1}, p_{j+2}, \dots, p_k$ merge, by $r_{j+1/2}$. The sequences P and R are sufficient for deriving the complete list of clusters at any linking length r . In fact, the segment p_i, p_{i+1}, \dots, p_j of the sequence P is an r -cluster if and only if $r_{i-1/2} > r$, $r_{j+1/2} > r$ and $r_{k+1/2} \leq r$, $k = i, i+1, \dots, j-1$. In other words, if all points would be located on a line with distances $r_{j+1/2}$, $j = 1, 2, \dots, n-1$ between neighboring points, the line would break into the sequence of all r -clusters after cutting of all segments larger than r . Obviously, the sequences P and R (each of length $n_p \times 4$ byte) is the most compact form to store the information about the whole hierarchy of friends-of-friends clusters.

After topological ordering we cut the MST using different linking lengths in order to extract catalogs of friends-of-friends particle halos. Note, that cutting a given MST is also a very fast algorithm. Typically we start with a linking length of 0.17 times the mean inter particle distance which corresponds roughly to objects with the virialization overdensity $\rho/\rho_{\text{mean}} \simeq 330$ at $z = 0$. Decreasing the linking length by a factor of 2^n ($n = 1, 2, \dots$) we get samples of objects with roughly 8^n times larger overdensities which correspond to the inner part of the objects of the first sample. With this hierarchical friends-of-friends algorithm we detect all substructures of halos. We are running the MST and FOF analysis independently on the dark matter and gas particles to compare their properties. At redshift $z = 0$ we have detected 975500 objects with more than 50 dark matter particles. All of these objects contain also gas particles. Running the MST and FOF analysis only over the gas particles we have detected 630800 objects with more than 50 gas matter particles which reflects the smoother distribution of the gas particles.

In Fig. 2 we show the mass function of the FOF-halos at different redshifts as total number of objects in the box. Already at redshift $z = 2$ first few objects with masses larger than $10^{14} h^{-1} M_{\odot}$ have been formed.

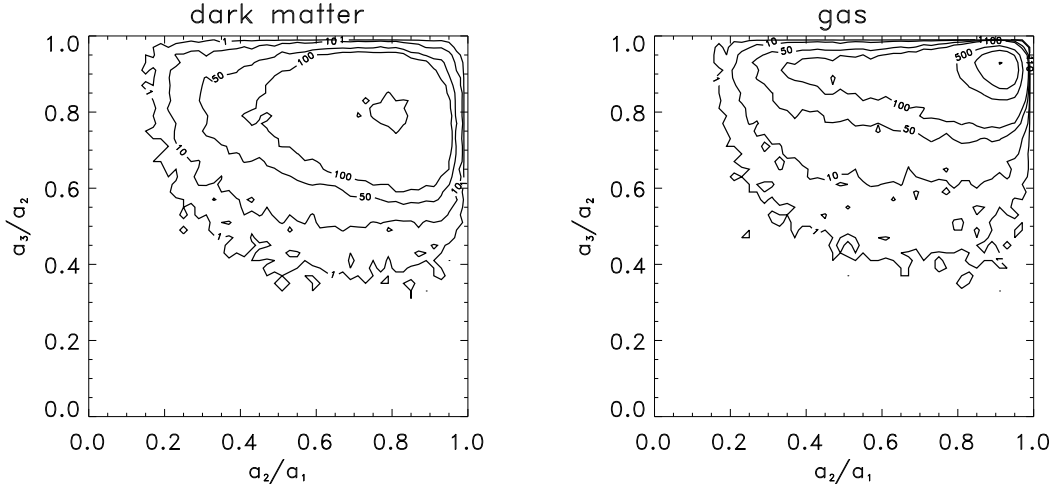


FIGURE 3. Left: Distribution of shapes of dark matter halos characterized by the ratio between main axes a_2/a_1 and a_3/a_2 . The contouring is done by halo numbers per bin. Right: The same for the corresponding gas halos.

Shape of Halos

It is well known that dark matter halos have triaxial shapes and tend to be prolate [4]. Their shape can be characterized by the three eigenvectors of their inertia tensor. Thus the shape of the objects is described by the three main axes $a_1 \geq a_2 \geq a_3$ of a three-axial ellipsoid. In Fig. 3 we show the distribution of shapes of halos with more than 500 particles. The interval between 0 and 1 has been divided into 50 bins of length 0.02. The contours show the number of halos per bin with the corresponding ratios of axes. Note, that the position of the maximum is mainly determined by the large number of low mass halos. In fact, due to the power law of the mass function about 50 % of the halos in this plot have particle numbers between 500 and 1000 and more than 90 % between 500 and 5000. The mean ratio of the axes of the dark matter and gas halos depends on mass [6]. Thus also the position of the maximum in the shape distribution shown in Fig. 3 will depend on the lower limit of mass assumed for the halos. However, the qualitative behavior does not depend on mass. The dark matter halos are triaxial and more prolate than oblate. The corresponding gas halos are only slightly triaxial with much higher axis ratios, i.e. they are more spherical.

Voids

In Fig. 1 (left panel) one can clearly see the filamentary structure of the dark matter distribution with large empty regions between the filaments. In the following we define voids as regions which do not contain any halo more massive than $10^{12} h^{-1} M_\odot$. Voids in the distribution of halos are found as described in [5]. In Fig. 2 (right panel) we show the cumulative volume occupied by those voids. The largest voids have radii of $18 h^{-1} \text{Mpc}$

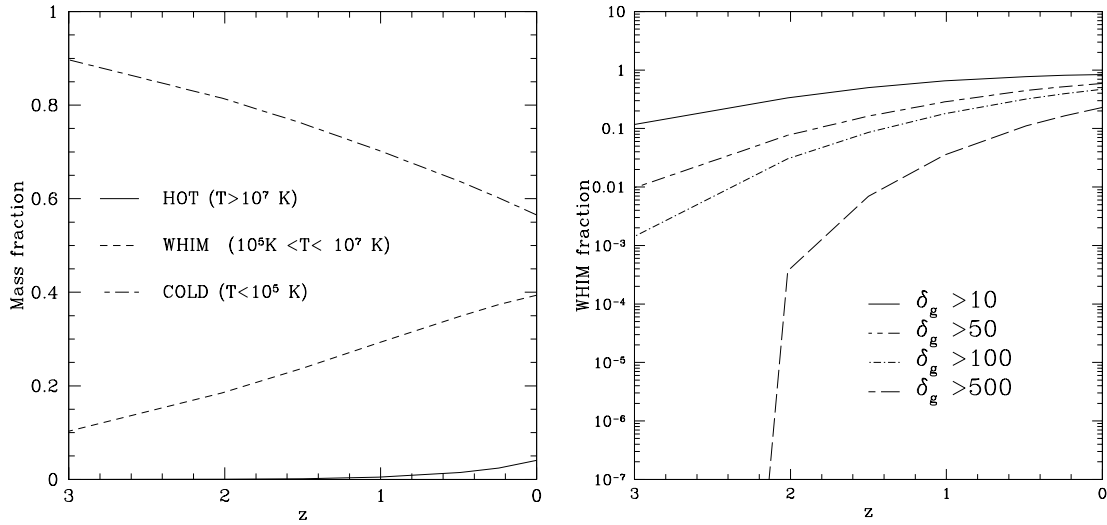


FIGURE 4. Left: Redshift evolution of the relative fractions of the different baryon components selected according to the temperature of the gas particles. Right: Redshift evolution of the WARM-HOT baryon phase for different overdensities.

and thus occupy only about 0.02% of the total volume. More than 14000 voids with radii larger than $5h^{-1}\text{Mpc}$ have been detected in the distribution of 505539 halos with masses larger than $10^{12}h^{-1}M_{\odot}$. They occupy a total volume of about 20 % of the simulation box.

Baryon Distribution

Due to the large number of gas particles that we have in this simulation, we are able to trace accurately the time evolution of the phase space ($T-\rho_{gas}$) distribution of baryons. We can then study the redshift evolution of the amount of gas at different temperatures inside the computational volume. In the left panel of Fig. 4 we plot this evolution for 3 different baryon components depending on the temperature: HOT ($T > 10^7 \text{ K}$), COLD ($T < 10^5 \text{ K}$) and WARM-HOT ($10^5 \text{ K} \leq T \leq 10^7 \text{ K}$). As can be seen in the figure, the amount of baryons in the WARM-HOT phase at present correspond to roughly 40 % of the total baryons in the simulation. They would represent a substantial fraction of the so-called missing baryons in the universe, as they would not be detected in X-rays due to their relatively low temperatures. In order to see how much of these WARM-HOT gas is located outside the dark matter halos, (*i.e.*, populating the low density filamentary structures or in voids), we show in the right panel of the same figure the evolution with redshift of the WARM-HOT gas located inside different local baryon overdensity thresholds. A baryon overdensity of order 60 corresponds roughly with virial overdensities for an isothermal sphere in the ΛCDM model ($\delta \sim 330$) [3]. Therefore, we can see in the figure that the fraction of baryons above certain overdensity increase rapidly at early times and becomes stable once the universe is dominated by exponential

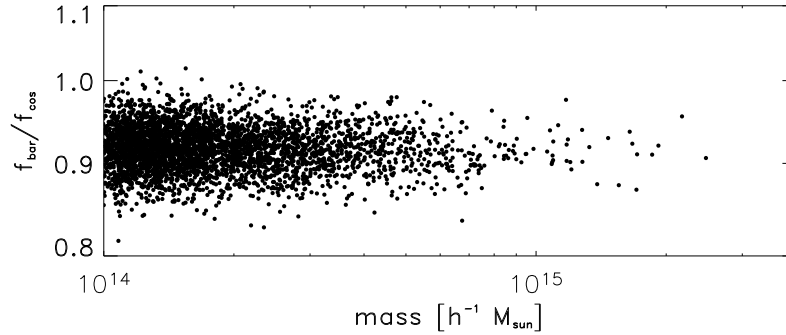


FIGURE 5. Baryon fraction in clusters

expansion ($z < 0.5$). This is in good agreement with the assumption that the baryons follow a log-normal density probability distribution [1]. We can also see from the figure that the amount of WARM-HOT baryons that live in overdensities lower than those inside virialized objects are of the order of 40%.

One of the aims of performing this simulation was to obtain a large database of galaxy clusters from which to study different observational properties. In Fig 5 we plot the baryon fraction for 4000 clusters in the simulation which have virial masses larger than $10^{14} h^{-1} M_{\odot}$. The baryon fraction is normalized to the cosmic mean ($\Omega_B/\Omega_M = 0.15$). As can be seen, the total content of baryons inside clusters is always smaller than the cosmic value for all clusters regardless of their mass.

ACKNOWLEDGMENTS

We would like to thank the Barcelona Supercomputer Center for allowing us to run the simulation described above during the testing period of MareNostrum. The analysis of this simulation has been done on NIC Jülich. We also thank Acciones Integradas Hispano-Alemanas and DFG for supporting our collaboration.

REFERENCES

1. F. Atrio, J. Mückel, *ApJ*, 643, 1 (2006)
2. S. P. Bhavsar, R. J. Splinter, *MNRAS***282**, 1461 (1996)
3. Davé, R., et al. *ApJ*, 552, 473 (2001)
4. A. Faltenbacher, S. Gottlöber, M. Kerscher, V. Müller, V., *A&A***387**, 778 (2002)
5. S. Gottlöber, E. Łokas, A. Klypin, Y. Hoffman, *MNRAS***344**, 715 (2003)
6. S. Gottlöber, G. Yepes, C. Wagner, R. Sevilla, astro-ph/0608289 (2006)
7. A. Klypin, S. Gottlöber, A. V. Kravtsov, A. M. Khokhlov, *ApJS***516**, 530 (1999)
8. D. N. Spergel, R. Bean, O. Dore', M. R. Nolte, C. L. Bennett, G. Hinshaw et al. astro-ph/0603449 (2006)
9. V. Springel, *MNRAS* 364, 1105 (2005)
10. V. Springel, et al. *Nature*, 435, 629 (2005)